Journal of Structural Geology 76 (2015) 22–34

Contents lists available at ScienceDirect

Journal of Structural Geology

journal homepage: www.elsevier.com/locate/jsg

A phenomenological numerical approach for investigating grain size evolution in ductiley deforming rocks

Andrew J. Cross [a, *], Susan Ellis [b], David J. Prior [a]

[a] Department of Geology, 360 Leith Walk, University of Otago, Dunedin 9056, New Zealand
[b] GNS Science, 1 Fairway Dr., Avalon, Lower Hutt 5011, New Zealand

ARTICLE INFO

Article history:
Received 30 October 2014
Received in revised form
29 March 2015
Accepted 3 April 2015
Available online 23 April 2015

Keywords:
Grain size evolution
Ductile deformation
Numerical model
Piezometer
Grain growth
Dynamic recrystallisation

ABSTRACT

The sizes of recrystallised grains in exhumed ductile shear zones are often used to infer conditions of deformation (i.e. stress, strain rate and temperature). Here we present a simple numerical method of calculating the dynamic evolution of grain size during ductile deformation. Our phenomenological method is based on the fact that the dynamic competition between grain growth and recrystallisation will drive grains towards a steady-state size. At each time increment, grain growth and reduction contributions are calculated, with magnitudes which depend on the difference between the current grain size and a desired steady-state grain size. In our models we use a recrystallised grain size piezometer to calculate the steady-state grain size for a given stress. Our numerical routine is incorporated into the SULEC finite element package, allowing us to explore spatial and temporal changes in grain size.

As a test, we compare model results to measured grain sizes in quartz layers thinned and recrystallised around rigid garnet porphyroclasts under simple shear dominated deformation in the Alpine Fault Zone of New Zealand. Numerical models are able to replicate observed grain size variations, with boundary conditions consistent with those constrained for the central Alpine Fault Zone.

1. Introduction

Below the seismogenic zone, increasing lithostatic pressures suppress brittle processes and increasing temperatures promote continuous distributed deformation in ductile shear zones, rather than on localised fault planes (Ramsay, 1980). Within these zones, deformation occurs either by the generation and motion of dislocations at high stresses, or by the diffusion of material under low stress conditions. In the boundary region between grain size insensitive dislocation creep and grain size sensitive diffusion creep, it is anticipated that a balance between grain growth and reduction mechanisms under steady-state deformation, prevents runaway rheological weakening by dynamic recovery and recrystallisation (De Bresser et al., 1998, 2001). Thus, the grain sizes of exhumed ductile rocks provide information on the magnitude of stress under which deformation occurred, which when combined with a rheological flow law can elucidate temperature and strain rate conditions, provided that limited post-deformational grain growth has occurred.

1.1. Grain size evolution

It is widely accepted that under steady-state conditions, an inverse relationship between recrystallised grain size and differential stress exists (Poirier, 1985). With increasing stress, the number of free dislocations in a material increases (Kohlstedt and Weathers, 1980; De Bresser, 1996) requiring recovery of dislocations by dynamic recovery and recrystallisation associated with grain size reduction. An expression for the relationship between recrystallised grain size, d and differential stress, σ was first derived for geological materials by Twiss (1977), based on the assumption that the ordering of dislocations into subgrain and recrystallised grain boundaries is an energetically favourable process. In the following years, many other 'paleopiezometric' relationships were derived primarily from experimental data on monophase aggregates, and commonly appear in the form:

$$d = A\sigma^{-b} \quad (1)$$

where A and b are empirical material constants.

* Corresponding author. Department of Earth and Planetary Sciences, Washington University in St. Louis, 1 Brookings Drive, St. Louis, Missouri 63130, USA.
E-mail addresses: ajcross89@gmail.com (A.J. Cross), s.ellis@gns.cri.nz (S. Ellis), david.prior@otago.ac.nz (D.J. Prior).

http://dx.doi.org/10.1016/j.jsg.2015.04.001
0191-8141/

The field boundary hypothesis of De Bresser et al. (2001) explains the development of a steady-state grain size by stating that under stable physical conditions, grains will evolve towards the boundary between grain size sensitive (GSS) and grain size insensitive (GSI) creep, where the ratio of strain rate contributions from dislocation and diffusion creep is unity.

Curiously, many laboratory-calibrated piezometers do not directly overlie the field boundary, yet lie sub-parallel to it (see Fig. 1 in Austin and Evans, 2009). Since the flow behaviour and recrystallisation of a crystalline material are both determined by dislocation dynamics and strain energy, both the flow law and piezometer should be strain rate and temperature dependent. However, in a series of deformation experiments on quartz, Stipp et al. (2006) found no water content, temperature or strain rate dependence of recrystallised grain sizes. Maybe this reflects the fact that only a relatively narrow range of conditions can be explored by laboratory experiments, although the paleowattmeter of Austin and Evans (2007, 2009), which is a stress, strain rate and temperature dependent alternative to grain size paleopiezometry, also predicts the discrepancy between the field boundary and steady-state grain size.

Further complications arise from the fact that while the De Bresser et al. (2001) model of grain size evolution is valid for monophase aggregates, in nature multiple mineral phases are often present together. In such a case, grain size evolution is restricted by the inhibition of grain boundary migration through a process called Zener pinning (Smith, 1948; Evans et al., 2001). Grain boundary pinning limits or entirely prevents the coarsening of grains, perturbing the dynamic balance of grain growth and recrystallisation, and leading to an unimpeded reduction in grain size and a transition to grain size sensitive deformation, so long as dislocations continue to be generated (Bercovici and Ricard, 2005; Warren and Hirth, 2006; Mehl and Hirth, 2008; Herwegh et al., 2011; Linckens et al., 2011). Grain boundary pinning has been proposed as essential to the development of plate tectonics, by enabling shear localisation to form plate boundaries in the early Earth (Bercovici and Ricard, 2013 and references therein).

1.2. Previous approaches to modelling grain size evolution

The idea of modelling grain size evolution in ductile shear zones is not a new one. Most previous approaches are based around the assumption that over time, a microstructure will evolve towards a steady state relationship between stress and grain size. While the evolution towards microstructural steady state is explained by the field boundary hypothesis of De Bresser et al. (2001), the numerical approaches applied in previous studies are quite varied and are summarised here.

Montési and Hirth (2003) approached the problem of modelling grain size evolution by modifying the field boundary hypothesis to address the discrepancy between the theoretical steady-state grain size-stress relationship of De Bresser et al. (2001) and empirically derived paleopiezometers (see Fig. 1 in Austin and Evans, 2007, 2009). In their study, Montési and Hirth allowed grain size to evolve towards a paleopiezometer (defined as in Eq. (1)), rather than the field boundary line. For grain sizes smaller than the stable grain size, the authors calculated grain size evolution using the standard grain growth equation (see Eq. (4) below), and for grain

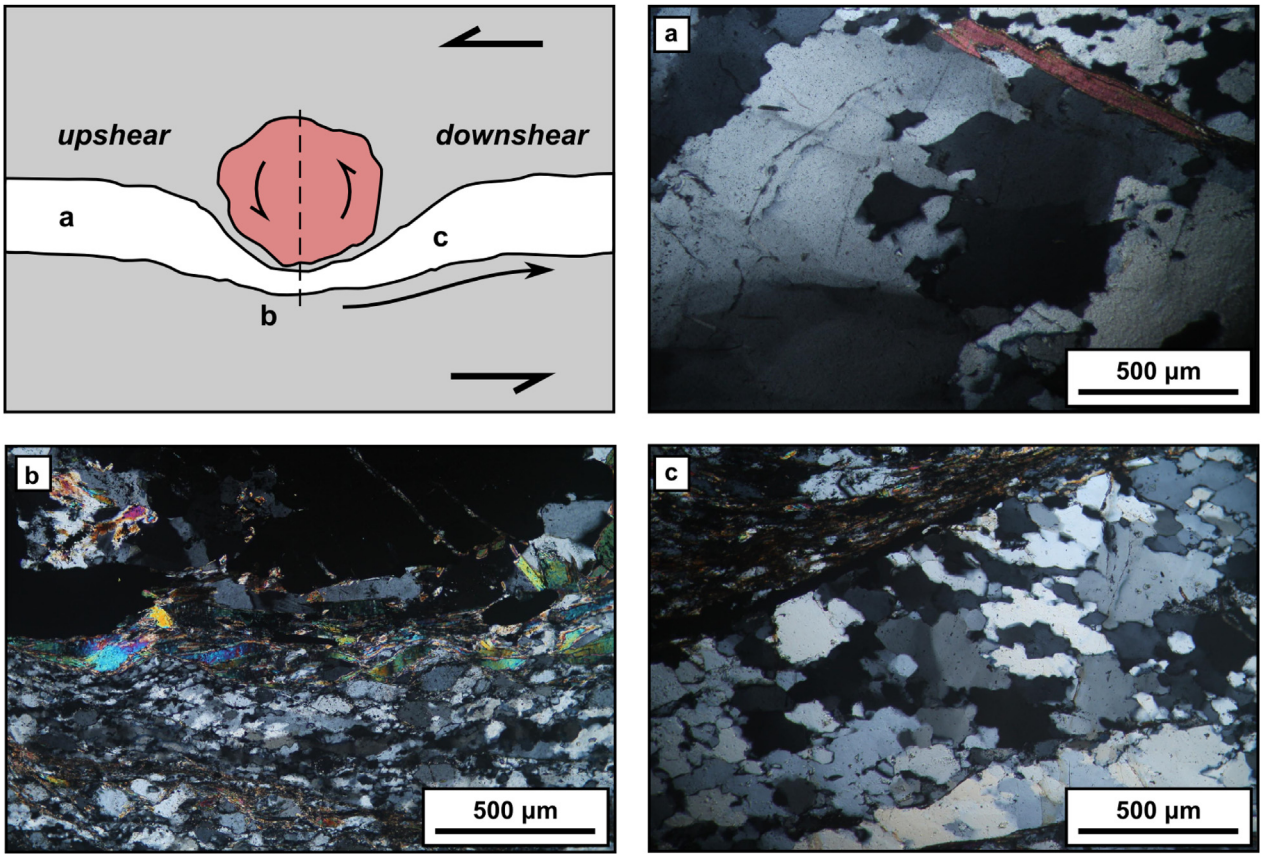

Fig. 1. Typical quartz microstructures along a deflected quartz layer. (a) Upshear of a garnet porphyroclast, quartz grains are large and internally distorted, with lobate boundaries indicative of rapid grain boundary migration. (b) Adjacent to the porphyroclast, grain sizes are significantly reduced. (c) Grains grow downshear of the porphyroclast, with polygonal shapes and little internal distortion.

sizes larger than the stable grain size, used a grain size reduction expression as follows:

$$\dot{d} = -\dot{\varepsilon}_r d/\dot{\varepsilon}_c \quad (2)$$

where ε_r is the strain rate accommodated by dislocation creep, and ε_c is a critical strain rate for microstructure evolution. This relationship is based on the assumptions of Derby and Ashby (1987) and Derby (1990), who suggest that new grains are statistically more likely to form, and thereby reduce the mean grain size, at faster strain rates and for larger grains. An advantage of the Derby and Ashby (1987) and Derby (1990) model, is that the piezometer grain size exponent, m (equivalent to b in Eq. (1)), and flow law exponent, n are dependent on each other, as predicted by De Bresser et al. (2001). However, De Bresser et al. (2001) compiled a range of m and n values, and found that the Derby and Ashby (1987) and Derby (1990) poorly replicated the empirical data.

Alternative approaches are implemented by the hybrid numerical modelling platform, Elle (see Piazolo et al., 2010 and references therein). In one approach, used by Jessell et al. (2005), grain size reduction is driven by the random insertion of high angle grain boundaries, based on the criterion $P = \varepsilon/2$, where the probability, P, of introducing a new boundary is greater for grains with a higher finite strain, ε. Piazolo et al. (2002, 2012) on the other hand, modelled recrystallisation by taking into consideration both the change in orientation due to crystal lattice reorientation and nucleation according to the work performed.

In contrast, Austin and Evans (2007, 2009) explored some of the kinetics of grain size reduction, by considering the balance of energy increase and dissipation under steady state. Their 'paleowattmeter' is a function of both stress and strain rate (i.e. the mechanical work applied to a volume), rather than just stress as in paleopiezometric relationships. This is more thermodynamically consistent with the inference that both the flow behaviour and steady-state grain size of a material is controlled by dislocation dynamics and strain energy. However, Austin and Evans acknowledge that their approach is essentially still a scaling relationship, and moreover, does not solve the discrepancy between the field boundary and piezometer.

A series of studies by Bercovici and co-authors (see Bercovici and Ricard, 2013 and references therein) uses a full thermodynamic treatment of grain size evolution to explore lithospheric shear zone localisation. These papers conclude that grain size pinning is a fundamental ingredient in rheological weakening, and was essential in the formation of plate boundaries in the early Earth. Other attempts to explore the influence of microphysical processes on grain size evolution include that of Herwegh et al. (2014), who also explore the localisation of deformation into steady state shear zones. In their study, the authors incorporate full thermodynamic coupling by considering the feedback between local production of heat and grain growth rates. In contrast to all previous studies, these authors incorporated the full thermo-mechanical range of grain size evolution starting from strain hardening, through strain softening (i.e. transient stages) and to a final steady state.

To explore the relationship between deformation conditions and grain size, we present a simple numerical method to interactively incorporate the grain size evolution of ductiley deforming rocks into a finite element mechanical model. Our numerical approach – which follows a methodology most similar to that of Montési and Hirth (2003) – relies on the fact that under steady-state conditions, grain size will evolve to a stable size in the boundary region between grain size sensitive and insensitive creep (De Bresser et al., 2001). Grain size reduction is driven by gravitation towards an energetically-favourable grain size, given by the paleopiezometer for a given stress, while grain growth is defined by the standard grain growth law. We employ a phenomenological approach in which we define an energetically favourable steady-state using empirical relationships (i.e. the paleopiezometer), rather than from first principles using complex thermodynamic and microphysical models. To test our numerical approach, we model variations in quartz recrystallised grain sizes around garnet porphyroclasts in shear. Similar natural samples, from the Alpine Fault zone of New Zealand, were recently studied and quantified using electron backscatter diffraction (EBSD) and TitaniQ thermobarometry (Cross et al., 2015). We are able to replicate, within error, the observed grain size variations at model conditions consistent with those anticipated for the Alpine Fault zone.

2. Grain size evolution in natural samples

To test the ability of our GSE routine to replicate natural microstructures, we have studied the variation in grain size in quartz layers deflected around rigid garnet porphyroclasts, where stress variations are predicted to be significant enough to produce a large grain size change in time and space. Our samples were collected from the mylonitic hanging wall of the Alpine Fault Zone, New Zealand.

2.1. Sample description and tectonic setting

The Alpine Fault is a 480 km long, oblique-reverse structure which represents the onshore segment of the Pacific-Australian plate boundary through New Zealand's South Island and forms the western extent of the uplifted Southern Alps. In its central section, the Alpine Fault dips at ~45° (Sibson et al., 1979; Norris and Toy, 2014), with a dextral strike-slip rate of 27 ± 5 mm yr^{-1} and uplift rates of 9–10 mm yr^{-1} (Norris and Cooper, 2001; Little et al., 2005; Norris and Toy, 2014), resulting in the exhumation of a 1 km-wide hanging-wall mylonite sequence formed by ductile deformation down-dip of the seismogenic brittle fault. The mylonite sequence contains a suite of protomylonites through to ultramylonites, with progressive smearing-out of pre-existing fabrics, grain size reduction and phase mixing. A kinematic analysis of lineations within the Alpine Fault zone (AFZ) mylonites by Toy et al. (2013) gave a best estimate of 3.5 for the maximum total pure shear strain, while total simple shear strains range from 11.7 (protomylonites) to 150 (ultramylonites). Thus, the majority of deformation experienced in the AFZ hanging wall is accommodated through simple shear.

Here we present data from three samples of garnet-bearing quartzofeldspathic Alpine Fault Zone mylonite, studied using electron backscatter diffraction (EBSD) to quantify grain size. The three samples chosen are all from the central Alpine Fault Zone, and include one mylonitic (STO-2-03) and two protomylonitic (TTR-01 and STO-2-08) samples, collected at horizontal distances of 400, 720 and 990 m from the Alpine Fault trace, respectively. Samples all exhibit systematic grain size reduction (by recrystallisation; Fig. 1a,b) and increase (by grain growth; Fig. 1b,c) in quartz layers deflected around garnet porphyroclasts during simple-shear dominated deformation, accompanied by rotation of a strong CPO and an increase in the number of grains deforming by rhomb and prism slip. Microstructural analysis and TitaniQ thermobarometry for these samples was recently completed (Cross et al., 2015), to constrain deformation conditions and inform our choice of model boundary conditions. We found that quartz microstructures predominantly record deformation accommodated through subgrain rotation recrystallisation (SGR) alongside rapid grain boundary migration (GBM), with some minor overprinting (evident through paleopiezometry) of continued SGR recrystallisation during exhumation and cooling, as creep decelerated. TitaniQ thermobarometry yields temperatures of 450–500 °C, which we suggest represent the cessation of widespread GBM, while

limited overprinting of GBM-microstructures implies rapid cooling from around the 500 °C isotherm to the brittle–ductile transition (at circa 350 °C). These temperatures lie within the temperature range reported for ductile deformation of the Alpine Fault zone mylonites (Toy et al., 2010 and references therein), and suggest strain rates consistent with those estimated near the mylonite–protomylonite transition (Norris and Toy, 2014).

2.2. Method: grain size analysis

EBSD mapping was carried out using an Oxford Instruments NordlysF EBSD camera fitted to a ZEISS SIGMA VP FEG-SEM, operating at 30 kV accelerating voltage and 90 nA beam current, at a working distance of 22 mm. Sample STO-2-03 was mapped in a Hitachi FE-SEM SU-70 SEM, operating at 20 kV and fitted with a Nordlys Nano EBSD detector. Microstructures were mapped by automatic beam rastering over a square grid with step sizes varying between 2 and 5 μm. We utilised automated stage movement to map the full lateral extent of quartz layer deflection. EBSD pattern acquisition and automatic indexing were done using the AZtec software by Oxford Instruments. 11 Kikuchi bands were automatically picked to determine crystallographic orientation for each pixel, with a Hough resolution of 70.

Raw EBSD maps were processed using the MTEX toolbox for MATLAB (Bachmann et al., 2011). The MTEX toolbox converts indexed pixels to grains using a Voronoi decomposition method (for more details see Bachmann et al., 2011). Grains are defined in this study as being encompassed by boundaries with misorientation angles of >10°, based on TEM observations in quartz by White (1977) and Shigematsu et al. (2006). We discarded grains smaller than 2 × 2 pixels in area to eliminate a skew in the grain size frequency distribution from misindexed pixels, and also removed grains based on the fraction of their area covered by indexed pixels (as in Cross et al., 2015). Recrystallised grains were isolated from a population of larger, relict grains, using a grain size threshold, defined by the 'knee' in a trade-off curve showing the number of grains versus grain size. Grain size is defined here as the diameter of a circle with the equivalent area of a given grain.

To represent variations in recrystallised grain size along quartz flow paths, the deflected quartz layer in each mapped sample was subdivided into several domains (Fig. 2a). Due to a systematic variation in grain size along each layer, domains had to be varied in area so that they each contained a similar number of grains (to allow statistical consistency), while being made small enough that microstructural evolution could be quantified using several domains along each layer. For each domain, we calculate the root mean square (RMS) recrystallised grain size for comparison to the piezometer data of Stipp and Tullis (2003) (Fig. 2b).

2.3. Results: grain size distribution

In all samples, we observe a modification of the microstructure adjacent to garnet porphyroclasts. Compositional layers defining the mylonitic foliation are thinned and grain size is reduced as flow is constricted around rigid porphyroclasts. As in Prior et al. (1999) and Bestmann et al. (2006), we assume flow paths to be subparallel to foliation. Here we define grains which are being transported towards the porphyroclast as being 'upshear', and those which have travelled around the porphyroclast and which are moving away as being 'downshear'.

Fig. 2a is an EBSD map with grains coloured according to their diameter. These data reveal a systematic variation in grain size in all samples; the largest grain sizes are situated away from the garnet porphyroclast, in the thicker part of each quartz layer, while the smallest grain sizes are always along the matrix–porphyroclast interface (see also Kenkmann and Dresen, 1998), in the region of maximum layer deflection and strain. These observations are supported by EBSD quantification of grain size for each domain (Fig. 2b), where recrystallised grains are typically 25–40 μm in diameter, and display a clear minima in the zone of maximum layer deflection.

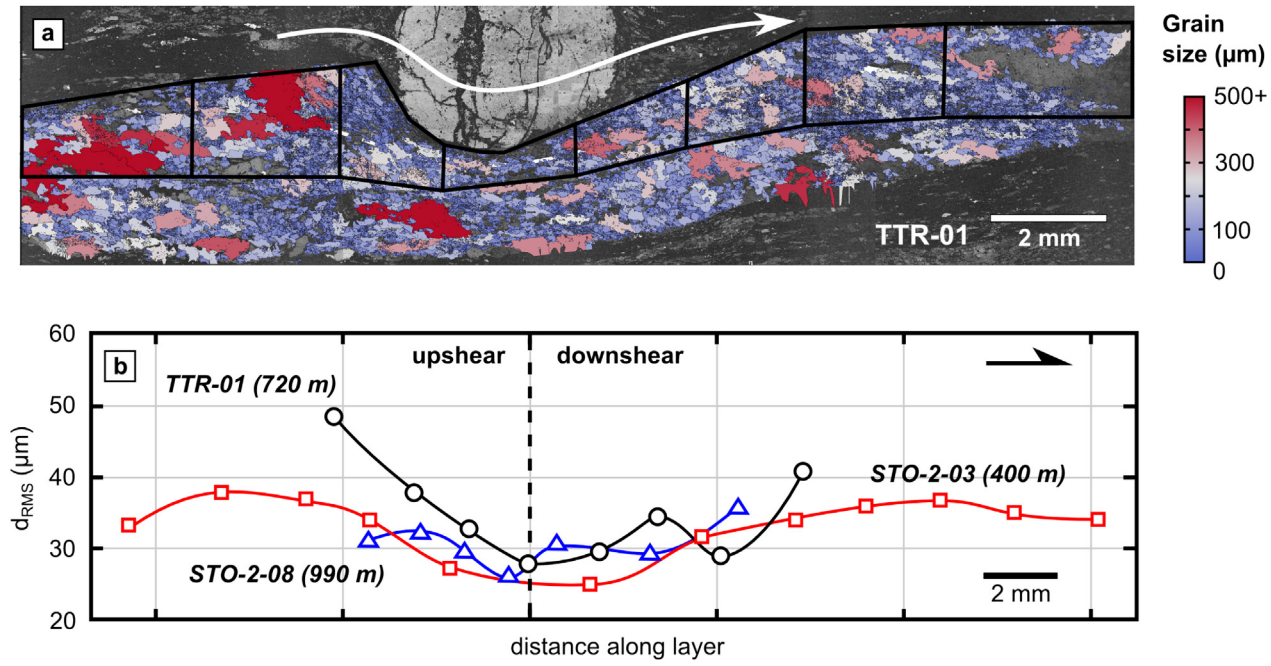

Fig. 2. (a) EBSD band contrast map of sample TTR-01, with grains coloured by their diameter. Black outlined regions are domains used for the quantification of grain size along the layer. Shear sense is top-to-the-left, giving a rightwards transport direction of the quartz layer at the base of the image. (b) Root mean square (RMS) grain sizes measured along each sample layer. Markers represent the centroid of each domain along a deflected quartz layer. The point of maximum layer deflection is marked by the vertical, dashed line and strongly coincides with the zone of maximum grain size reduction. Standard deviations of grain size distributions at each point are typically 5–15 μm.

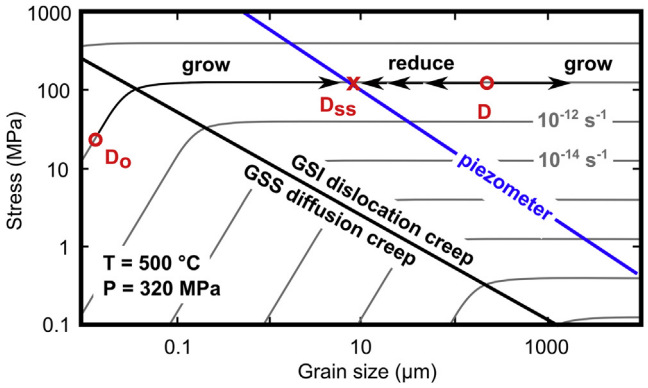

Fig. 3. A deformation mechanism map of log stress, σ versus log grain size, D for quartz, based on the rheological data of Brodie and Rutter (2000) and Hirth et al. (2001). Lines of constant strain rate are shown in grey and curve over the field boundary region approximated by a line at which contributions to deformation from dislocation and diffusion creep are equal. In the GSI field, both grain growth and reduction mechanisms are active, while in the GSS field there is no mechanism for recrystallisation. D_o = grain size before grain growth; D = grain size before grain size reduction; D_{ss} = steady state grain size dictated by the piezometer.

3. Numerical approach

Grain size evolution is a function of competing grain growth and reduction (i.e. recrystallisation) processes. Over a given time interval, net grain size change is a product of grain growth and reduction contributions:

$$\Delta D = \Delta D_{\text{grow}} - \Delta D_{\text{reduce}} \tag{3}$$

Static grain growth is driven by the reduction of Gibbs free energy along grain boundaries (Evans et al., 2001) and follows an inverse-logarithmic function as grain boundary curvature, and therefore Gibbs free energy, is progressively reduced (Humphreys and Hatherly, 2004):

$$\Delta D_{\text{grow}} = \left(F_g K_o e^{(-Q/RT)} \mathrm{d}t + D_o^p\right)^p - D_o \tag{4}$$

where K_o is a constant, p is the growth exponent, Q is the activation energy, R is the gas constant, T is absolute temperature, ΔD_{grow} is the change in grain size over the time interval dt and D_o is the initial grain size at $t = 0$. F_g is a grain growth efficiency factor which we vary between 0 and 1 to effectively turn grain growth off or on, respectively.

The kinetics of grain size reduction by dynamic recrystallisation are less well constrained. Most approaches to computing the rate of dynamic recrystallisation (Hall and Parmentier, 2003; Montési and Hirth, 2003; Austin and Evans, 2009; Piazolo et al., 2010) are based on the assumption that recrystallisation is a statistical phenomenon whereby the rate of grain boundary production is faster in larger grains, and at higher strain rates where the rate of dislocation production is greater (Derby and Ashby, 1987). In this study we use the following scaling law based on the same assumptions, where the driving force for recrystallisation at a given stress is the difference between the current grain size, D, and the stable (i.e. energetically-favourable) grain size, D_{ss}, defined by the paleopiezometer:

$$\Delta D_{\text{reduce}} = (D - D_{ss})^l K_o e^{(-Q/RT)} \mathrm{d}t \tag{5}$$

where l is a reduction exponent similar to the growth exponent n in Eq. (4), K_o is a constant, and Q is the activation energy for which we assume the same kinetic parameters as in the grain growth law ($K_o = 4.96\ P^{2.34}$; $p = 3.2$). While we acknowledge that the kinetics of recrystallisation may be different to those of grain growth, the models presented below show that the rate of grain size reduction is rapid enough that, as stresses increase, grain sizes maintain a stable size along the paleopiezometer, without making an excursion into the GSI field. The kinetic parameters used here to describe recrystallisation yield a grain size reduction rate that is sufficiently rapid to satisfy this criteria.

Though not explicitly expressed in Eq. (5), the grain size reduction rate in our method is, like the paleowattmeter, both strain rate and temperature dependent. For a given grain size within the GSI field, the distance from the piezometer ($D - D_{ss}$; the driving force for recrystallisation) is smaller at lower stresses and therefore lower strain rates or higher temperatures (Fig. 5).

3.1. Implementation of grain size evolution approach

Based on the relationships defined above, we have incorporated a new grain size evolution (GSE) routine into a numerical code (SULEC) which solves the Stokes equations for the momentum of creeping flows (Ellis et al., 2011; Buiter and Ellis, 2012; Grigull et al., 2012). Our routine computes the net change in grain size, ΔD from grain growth and recrystallisation contributions at each timestep (Eq. (3)), generating feedback with flow stress by passing the new grain size to the next timestep (see Fig. 4 for further details). By using tracer particles (discussed further below), we can track the evolution of grain size along a flow path through the finite-element mesh.

At each timestep and at each discretised point in the model, SULEC passes a value of stress (calculated by the GSI and GSS flow laws) to the GSE routine, which calculates a grain growth contribution, ΔD_{grow}, regardless of active creep mechanism, since grain growth is active under all conditions (Fig. 3). Next, a steady-state grain size, D_{ss} is calculated according to the piezometer for the given stress. If the grain size at the start of the timestep is greater than D_{ss}, GSI creep is considered active and a grain size reduction contribution, ΔD_{reduce} is subtracted (Eq. (5)). The final grain size, after growth and reduction, is passed out of the routine and used in the grain size dependent composite flow law, to calculate stress in the next timestep. Timesteps were chosen to be small enough so that the sequential calculation of ($\Delta D_{\text{grow}} + \Delta D_{\text{reduce}}$) did not depend significantly on the order in which each increment was added.

4. Modelling grain size evolution

4.1. Model setup and boundary conditions

We model the flow of viscous quartz around a rigid porphyroclast using an Eulerian grid through which materials and material properties are advected using tracer particles. Equal and opposing velocity boundary conditions are applied along the top and bottom edges, giving a simple shear geometry. Since deformation in the Alpine Fault zone is simple-shear dominated (Toy et al., 2013), we do not impose a flattening strain component, and assume that the observed microstructures were formed entirely with a rotation axis perpendicular to the plane of interest (the X–Z plane in a standard reference frame). Table 1 summarises the model parameters described below.

4.1.1. Strain rate and temperature

Boundary velocities are scaled to the grid height (i.e. shear zone width) to yield shear strain rates between 10^{-14} s^{-1} and 10^{-10} s^{-1}. This range of strain rates is wider than that expected for the Alpine

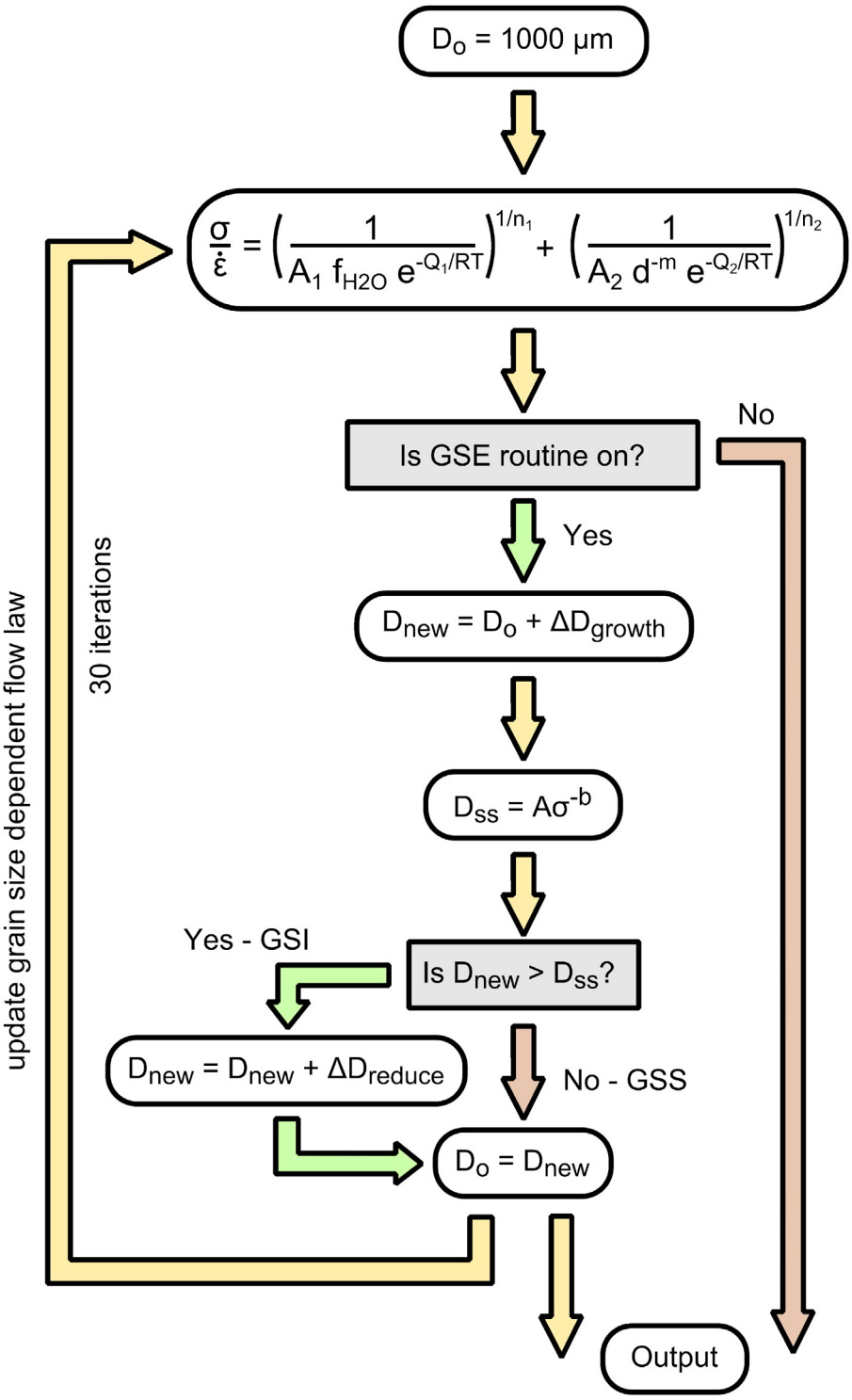

Fig. 4. Flow chart for the grain size evolution (GSE) subroutine. Initial grain size and stress (calculated from the dislocation creep (subscript 1) and diffusion creep (subscript 2) flow laws) are fed into the GSE routine, which calculates and outputs a new grain size to use in the next iteration.

Fault zone (10^{-13} s^{-1}–10^{-11} s^{-1}) based on maximum shear strains accumulated in the AFZ mylonites over the past 5 Myr (Norris and Cooper, 2003; Toy et al., 2013; Norris and Toy.2014).

SULEC also allows boundary temperatures to be defined to give vertical and lateral geothermal gradients. For our millimetre-scale model space, we assume isothermal conditions in the range of 400 °C–600 °C, to encompass the conditions of creep given for the AFZ mylonites (Vry et al., 2004; Toy et al., 2010). Though the Alpine Fault mylonites experience cooling through time (as a result of syn-deformational exhumation), we assume that the measured recrystallised grain sizes reflect only the last increment of deformation before creep ceased entirely, since quartz in our natural samples appears to have been quenched rapidly (Cross et al., 2015). We also neglect the effects of shear heating in the models shown

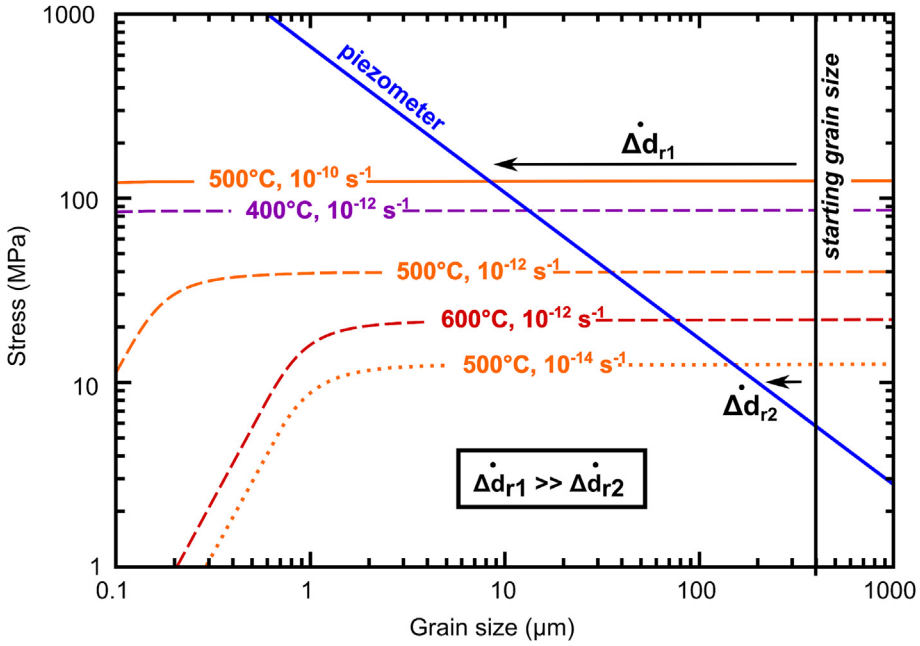

Fig. 5. Comparison of recrystallisation driving forces ($D-D_{ss}$) at various temperature and strain rate conditions. At 500 °C, the rate of grain size reduction ($\Delta d_r/dt$) is much greater at 10^{-10} s^{-1} than at 10^{-14} s^{-1}, for a fixed starting grain size.

here. Tests using a shear heating efficiency of 1 were used to verify that shear heating does not produce a significant thermal perturbation around the grain. At our optimal model conditions, heat production is 4.2×10^{-5} at most (along the porphyroclast interface), corresponding to a thermal perturbation of <0.01 °C; far less than the 1 °C proposed to result in shear localisation (Peters et al., 2015).

Table 1
Model parameters.

Parameter	Value
Gas constant, R (J K^{-1} mol^{-1})	8.314
Density (kg m^{-3})	2700
Temperature, T (°C)	400–600
Strain rate, $\dot{\varepsilon}$ (s^{-1})	10^{-10}–10^{-14}
Initial grain size, D_o (μm)	1000
Element width in model mesh (μm)	50–100
GSI rheology (*Hirth et al., 2001*):	
Pre-exponent, A (MPa^{-n} s^{-1})	$10^{-11.2}$
Stress exponent, n	3
Grain size exponent, m	0
Activation energy (kJ mol^{-1})	135
GSS rheology (*Brodie and Rutter, 2000*):	
Pre-exponent, A (MPa^{-n} s^{-1})	$10^{-0.2}$
Stress exponent, n	1
Grain size exponent, m	−2
Activation energy (kJ mol^{-1})	220
Grain size reduction parameters:	
Pre-exponent, K_o (m^{-p} s^{-1})	4.96 $P^{2.34}$
Activation energy , Q (kJ mol^{-1})	215
Reduction exponent, p	3.2
Grain growth parameters:[a]	
Pre-exponent, K_o (m^{-p} s^{-1})	4.96 $P^{2.34}$
Activation energy , Q (kJ mol^{-1})	215
Growth exponent, p	3.2
Quartz piezometer (*Stipp and Tullis, 2003*):	
Pre-exponent constant, A	3631
Exponent, b	1.26

[a] Derived by Wightman et al. (2006) from the quartz data of Tullis and Yund (1982)

4.1.2. Rheology

We apply the quartz flow laws of Brodie and Rutter (2000) and Hirth et al. (2001) to define the composite thermally-activated diffusion and dislocation creep laws for rheology of the matrix, while a high frictional cohesion and viscosity is given to the porphyroclast to make it rigid. The matrix and porphyroclast share nodes of the Eulerian grid, resulting in a fully-coupled interface, as anticipated by Masuda and Ando (1988). The Hirth et al. (2001) dislocation creep flow law was used (rather than the Brodie and Rutter (2000) dislocation creep flow law) because it was constrained under natural conditions and was shown in Cross et al. (2015) to give more appropriate predictions of strain rate in the AFZ mylonites. Moreover, the Hirth et al. flow law is sensitive to the pressure-and temperature-dependent fugacity of water. For each temperature modelled, we calculate corresponding pressures and water fugacities using the modified (from Toy et al., 2010) Alpine Fault geotherm presented in Cross et al. (2015), assuming a rock density of 2700 kg m^{-3}.

4.1.3. Porphyroclast geometry and initial position

A dense distribution of Lagrangian tracer particles (of which a defined number are randomly distributed within each Eulerian grid cell) are used in SULEC to replicate the geometries of porphyroclasts observed in our natural samples. The MTEX open-source texture analysis toolbox for MATLAB contains a grain detection algorithm for EBSD data (Bachmann et al., 2011), which allows us to access the $x-y$ coordinates for the grain boundary of a specific grain. By obtaining the grain boundary coordinates of a porphyroclast, we can interpolate its geometry onto tracer particles via a Delaunay triangulation algorithm built into MATLAB. To reduce the computation time, we remove any internal boundaries and reduce the number of boundary nodes by a factor of ten, to decrease the number of triangles in the mesh without compromising the grain geometry or introducing artificial stress concentrations at porphyroclast vertices.

In our models, the garnet porphyroclast is modelled as a highly viscous inclusion that effectively acts as a rigid object and therefore

passively rotates. Since we want the porphyroclast to have the same orientation as in the natural sample on the final iteration, we run a set-up phase of our model with a reversed shear sense, in order to back-rotate the porphyroclast. Essentially, we ran the model in reverse for 30 iterations and captured the resultant porphyroclast geometry, which was then fed back into the main model phase.

4.2. Model procedure

During the main phase of modelling, the correct shear sense is used and run for 30 iterations as in the set-up phase. At this stage, a tracer particle is placed at specified starting coordinates and used to track changes in stress and grain size during shear around the porphyroclast. Since grain size is advected with each Lagrangian particle, this tracer particle can be thought of as a single grain, which grows and reduces in size freely in response to the changing stress field.

Material and rheological properties at every Eulerian grid node are written to a file at the end of each timestep. We use the Paraview open-source visualisation package (http://www.paraview.org) to view the evolution of these properties (such as differential stress and grain size) over the duration of the model run. Fig. 6 shows an example of model output at one timestep. The Lagrangian tracer particle used to track grain size evolution writes to a separate file which gives particle coordinates and an associated grain size at each timestep. We use this information to compare grain size evolution under various model boundary conditions (Fig. 7).

4.3. Model sensitivity

To investigate the importance of the model parameters in determining stress and grain size magnitudes and gradients we performed a series of sensitivity tests, in which one parameter was varied while the rest were kept constant. We explored the sensitivity to variables with the greatest degree of uncertainty and error, namely the deformation conditions (temperature and strain rate) and grain growth rate.

4.3.1. Strain rate and temperature

Strain rates experienced by the Alpine Fault zone mylonites vary laterally by an estimated two orders of magnitude (increasing towards the Alpine Fault trace), and temperatures by up to 200 °C due to exhumation during deformation (Norris and Cooper, 2003;

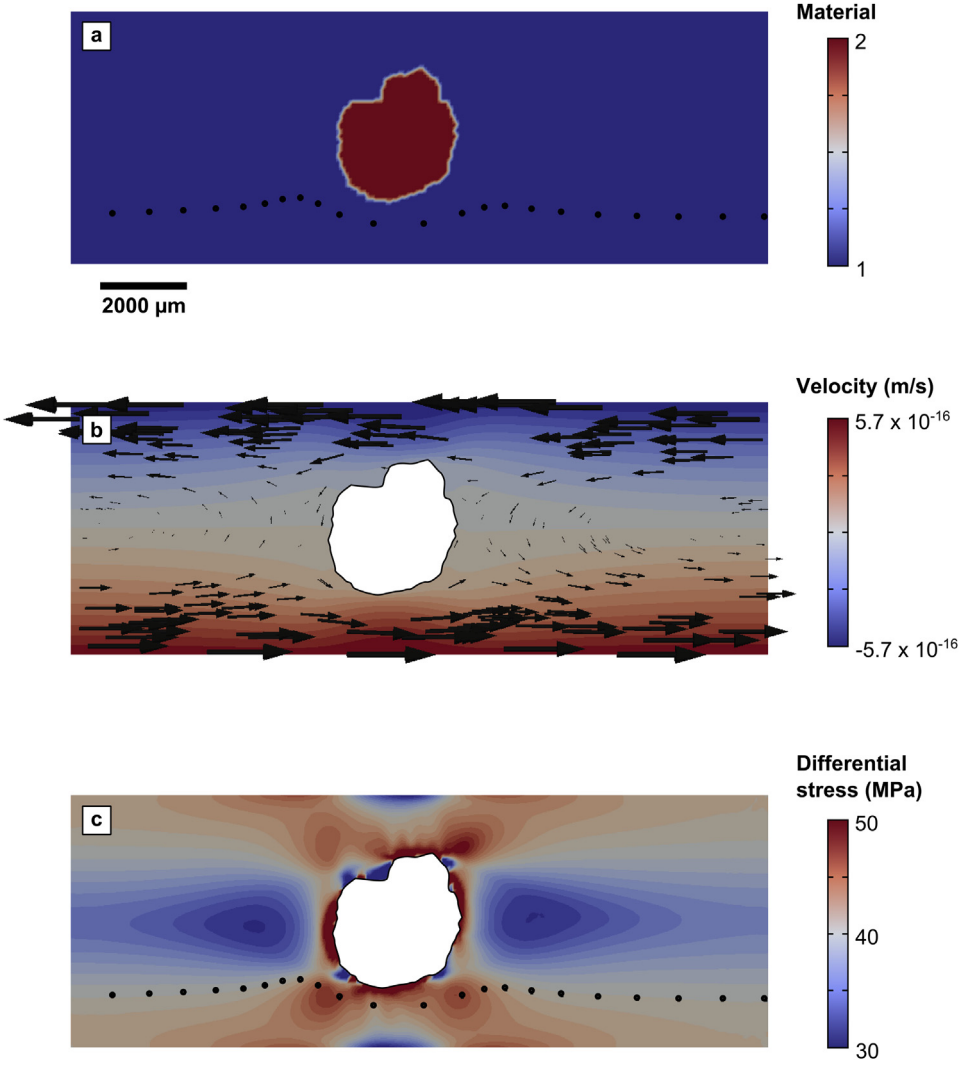

Fig. 6. SULEC model setup for (a) material geometry and (b) velocity, with a sinistral shear sense. The geometry of the rigid central porphyroclast shown here is taken from sample TTR-01. (c) At a shear strain rate of 4×10^{-13} s^{-1} and temperature of 475 °C, resultant differential stresses range from 30 to 50 MPa. Black dots represent the position of the tracer particle at each timestep, moving from left to right. Plotted in Paraview (http://www.paraview.org).

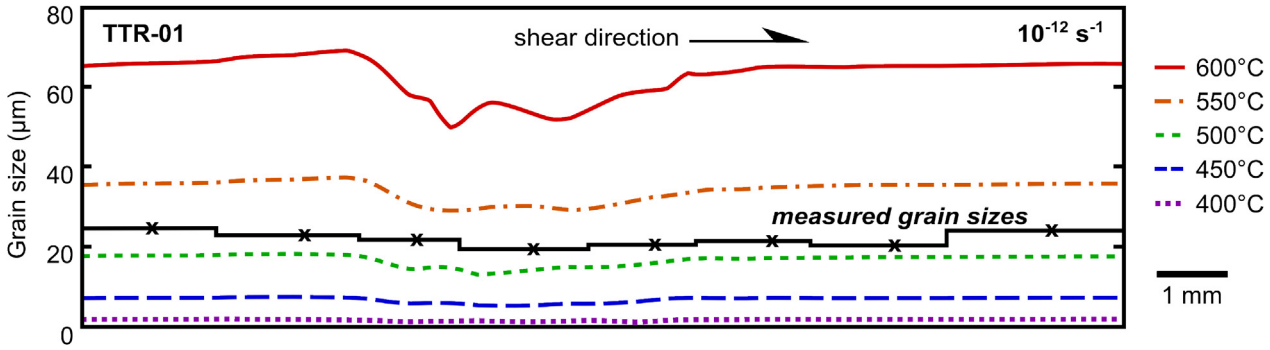

Fig. 7. Predicted grain size transects at a strain rate of 1×10^{-12} s^{-1} and various temperatures, compared with measured RMS grain sizes (black line) for sample TTR-01. Line segments for measured data correspond to the domains described above and outlined in Fig. 2a, while domain centroids are shown as crosses.

Vry et al., 2004; Toy et al., 2010, 2013; Norris and Toy, 2014). Though we can approximate the conditions of deformation in our samples based on the proximity (horizontal distance) of each sample to the brittle fault trace, we explore all anticipated conditions in our models. In fact, we widen the range of strain rates modelled to address the possibility that our samples record deformation at sub-seismic strain rates immediately below the seismogenic zone.

Fig. 7 compares the predicted grain size transects (obtained from the tracer particle) with the measured grain sizes in sample TTR-01 for various temperatures, and at a strain rate of 1×10^{-12} s^{-1}. The measured grain size data are represented over the width of each sample domain (as outlined in Fig. 2), with the domain centroids marked by a cross. For each sample domain, we calculate the difference between the model-predicted and measured grain sizes, and take the mean of these differences to yield the mean grain size misfit for each set of boundary conditions. To compare the mean misfits across a range of both temperature and strain rate, we represent these values as a contour plot in Fig. 8.

Our sensitivity tests reveal a zone of increasing temperatures and strain rates, which fit the measured grain size data equally well. Despite this non-uniqueness, we are able to place *a priori* constraints on the optimum model setup, based on estimates of strain rates and temperatures in the Alpine Fault Zone mylonites. Temperatures recorded by quartz in the AFZ mylonites range between 450 and 500 °C (Cross et al., 2015). At these temperatures, the optimum strain rates (as revealed by our sensitivity tests) are in the range of 8×10^{-14} s^{-1} to 7×10^{-13} s^{-1}. Given that these samples were collected close to the mylonite–protomylonite transition in the AFZ hanging wall, where shear strains accumulated over 5 Ma are estimated as 12–22 (Norris and Cooper, 2003), we would expect shear strain rates to lie between 3.8×10^{-13} s^{-1} and 7.0×10^{-13} s^{-1}. This encouraging overlap in strain rates demonstrates that our measured grain size distributions are best fit at model conditions consistent with strain rates and temperatures reported for the Alpine Fault zone.

4.3.2. Grain growth rate

In nature, mylonitic rocks commonly contain well-mixed multiple phases, which are expected to inhibit grain boundary migration through Zener pinning, and thereby limit the rate of grain growth (Olgaard and Evans, 1986; Evans et al., 2001; Bercovici and Ricard, 2012). Though we have tried to avoid grain boundary pinning by picking samples of single-phase quartz layers, it is nonetheless important to explore the effects of varying grain growth rates in our models. To this end, we vary the grain growth efficiency factor outlined in Eq. (4) between 0 and 1, where 0 represents fully pinned grain boundaries incapable of growth, and 1 represents normal grain growth rates, as given by Wightman et al. (2006) from the static annealing data of Tullis and Yund (1982). The effects of varying the grain growth efficiency factor, F_g can be seen in Fig. 9. With decreasing grain growth efficiency, the degree of asymmetry increases such that grains downshear of the garnet remain small in size and out of steady-state.

Model results for each sample are shown in Fig. 10, with varying rates of grain growth. Most models show a reasonable fit to the data, within error, though it is clear that the models in which grain growth is slower (i.e. 10%) are most strongly asymmetric and do not fit the data. The best fit is given by a 100% grain growth rate; that is, the static annealing rate derived from the Tullis and Yund (1982) data.

5. Discussion

5.1. Comparing numerical and natural grain size evolution paths

Fig. 10 shows that, to first order, the natural grain size data are well fit by our numerical models. The predicted grain size evolution paths all show an initial stage of rapid grain size reduction upshear of the garnet porphyroclast, which fit the natural data well. This fit implies – given the rapid rate of grain size reduction imposed in our models – that recrystallisation is rapid enough to keep grain sizes at a stable size under increasing stresses, such that the microstructure doesn't deviate from the paleopiezometer.

Downshear of the porphyroclast, the natural data are best fit by a grain growth efficiency of 1, suggesting that grain boundaries are fully mobile and not pinned. However, the rate of grain growth in the model appears slower than the rate of grain size reduction, yet fits the natural data equally well. This trend is evident in all three natural samples (see Fig. 2a for example), where the largest grains are always situated directly upshear of the garnet porphyroclast, and grains of an equal size are not observed downshear (at least over the same length scale). Perhaps then, this reflects the fact that grain growth in our natural samples operates at a slower rate than recrystallisation.

Finally, the range of grain sizes predicted by the models is narrower than in nature. This can be easily explained since, in the natural data, grain sizes are averaged over a broad domain, rather than being calculated at a discrete point, as in the case of the Lagrangian tracer particle. This is particularly important to note for grain sizes calculated near the porphyroclast, since the smallest grain sizes are located at stress concentrations along the porphyroclast–matrix interface, and are not 'seen' by the tracer particle in our models (Fig. 9).

5.2. Discontinuous versus continuous deformation

Quartz microstructures and titanium concentrations indicate that the majority of ductile creep in quartz ceased between the

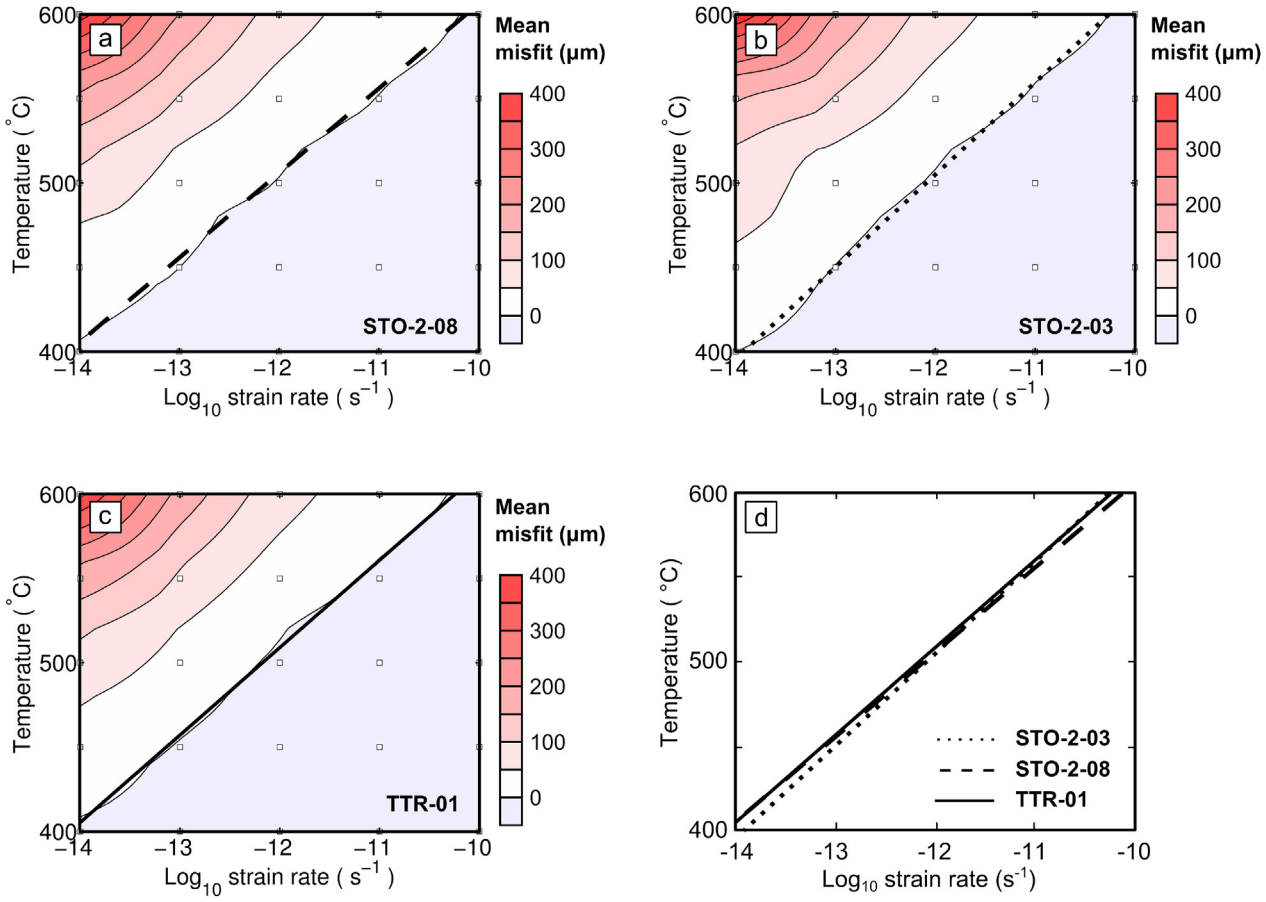

Fig. 8. Contour maps of mean misfit (μm) between predicted and measured grain sizes (Fig. 7) in each sample, for various temperature and strain rate conditions. White squares mark the temperature and strain rate combinations tested in SULEC. The misfits at each of these points are used in the construction of contours. Red colours indicate an overestimation of model grain sizes, while blue colours represent underestimation. The optimum model setup is approximated by a linear trend of increasing temperature and strain rate in each case. A comparison of optimum setups for each sample is shown in Figure (d). (For interpretation of the references to color in this figure legend, the reader is referred to the web version of this article.)

450–500 °C isotherms. This is supported by the fact that our measured grain sizes are well replicated by the grain size evolution routine presented here, at strain rates consistent with continuous creep at these temperatures. However, some authors have previously proposed that the middle crust can become elastically loaded by upper crustal earthquakes, producing high stress microstructures (e.g. Küster and Stöckhert, 1999; Ellis and Stöckhert, 2004); strain rates may exceed 10^{-10} s^{-1} under such circumstances. We must therefore address the possibility that our samples record discontinuous, sub-seismic deformation.

In Fig. 8, we showed the misfit to the grain size data from models at the expected sub-seismic conditions. The misfit analysis shows that at low temperatures and fast strain rates, we would expect our models to underestimate the observed grain sizes. In other words, the natural grain sizes are too coarse to have been produced by sub-seismic deformation. The fact that few 120° triple junctions are present in our samples (Fig. 1) also rules out the possibility that small grains were formed at sub-seismic conditions and subsequently grew to produce the measured grain sizes. On this note, quartz recrystallised grain sizes were extensively studied in the Alpine Fault zone by Kidder et al. (2014), who consistently found a population of recrystallised grains as small as 4 μm, which they attribute to elastic-loading of the mid-crust by earthquakes. Such grains are distinct from those modelled in this study, which we suggest represent continuous deformation at ambient strain rates (~10^{-13} s^{-1}).

5.3. Choice of steady-state relationship

It is important to also consider the dependence of our results on the piezometer used, to which grain sizes gravitate in our method. Though the Stipp and Tullis (2003) piezometer is widely used for calculating steady-state stress from grain size (e.g. Gueydan et al., 2005; Behrmann and Seckel, 2007; Kidder et al., 2012), we plot a comparison to other grain size-stress relationships in Fig. 11.

The grain size-stress relationships compared in Fig. 11 are all of similar gradients in log–log space, sub-parallel to the field boundary line as calculated from the Hirth et al. (2001) and Brodie and Rutter (2000) quartz flow laws. These relationships lie closely together within the dislocation creep field, though for a given range of recrystallised grain sizes, the Twiss (1977) piezometer will yield the greatest range in estimated stresses.

At a given grain size, it is also possible to independently evaluate the range in estimated stress from the various piezometers. For 40 μm grains, representative of background deformation in the samples studied here, the median stress estimate (36 MPa) is given

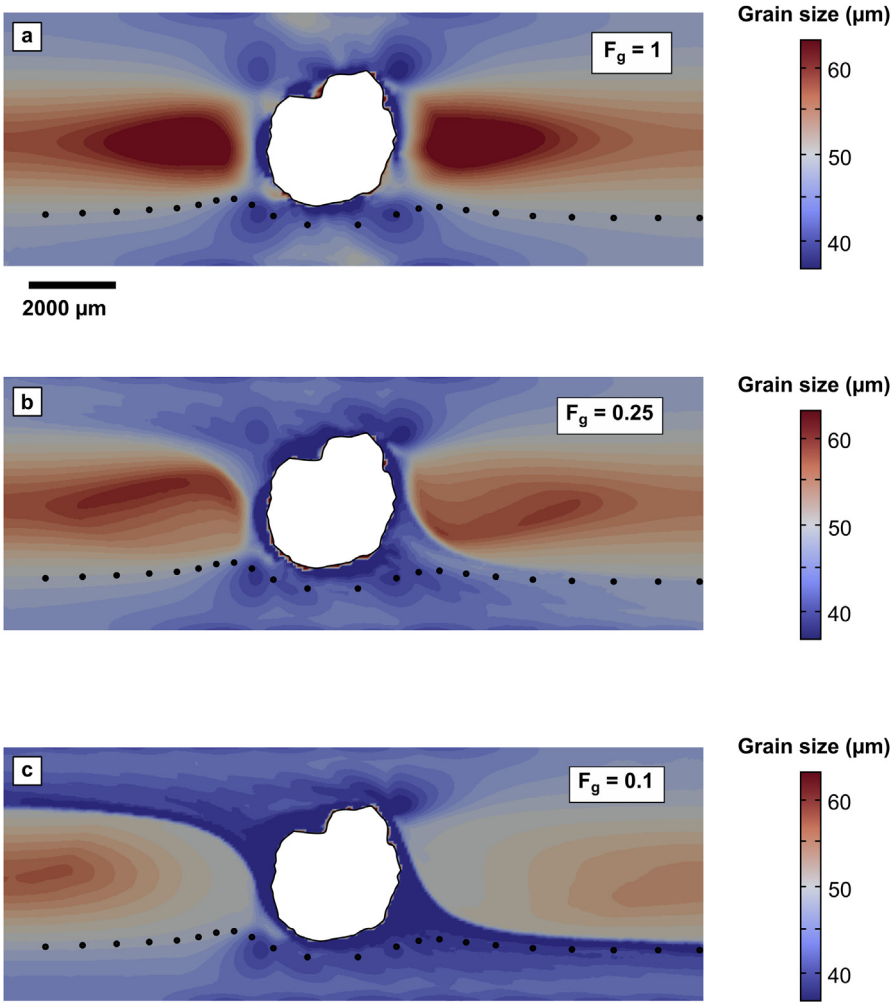

Fig. 9. Grain size distributions in SULEC at grain growth efficiencies of (a) 1, (b) 0.25 and (c) 0, where 0 represents prohibited grain growth and 1 allows normal rates of grain growth as given by Tullis and Yund (1982). Black dots mark the position of the tracer particle (used to track grain size evolution) at successive timesteps. Plotted in Paraview (http://www.paraview.org).

by the Stipp and Tullis (2003) piezometer and corresponds to a strain rate of 3.43×10^{-13} s^{-1}. From the paleowattmeter and Twiss piezometer, stresses range from 24 to 55 MPa respectively, equating to strain rates of 6.77×10^{-14} to 1.87×10^{-12} s^{-1}, at a temperature of 500 °C. Since these strain rates are at the extremes of the strain rate range expected for the Alpine Fault Zone mylonites, we are confident that the Stipp and Tullis (2003) piezometer – which gives the median values of stress and strain rate – is an appropriate relationship to apply in this case.

5.4. Application to ductile shear zones

The model results presented in this paper show that our numerical treatment of grain size evolution is able to replicate grain size observations in natural mylonites with reasonable accuracy. Sensitivity tests provide optimum boundary conditions which match exactly the well-constrained temperatures and strain-rates in the Alpine Fault Zone. This is a testament also to the validity of extrapolating laboratory-derived flow laws and paleopiezometers to natural rocks, at least in the case of quartz.

Though we have presented here a rather simple deformation geometry by choosing small samples of monophase quartz layers, our results give us confidence that the same method may be tested against larger scale or more complex systems in which boundary conditions (namely temperature and rate of deformation) change through time. The ability to vary the relative rates of grain growth and reduction may be of particular importance in the case of multiphase rocks, where grain boundary pinning is likely to be significant in reducing the rate of grain growth.

6. Conclusions

We have presented a simple numerical method for modelling grain size evolution during ductile deformation. Our method is based on a modified field boundary hypothesis, in which the dynamic competition of grain growth and recrystallisation drives evolution towards a piezometer under steady state conditions. Using our numerical approach we are successfully able to reproduce grain sizes measured in quartz layers undergoing recrystallisation during deflection around rigid garnet porphyroclasts, contained in Alpine Fault Zone mylonites. Moreover, we are able to get an optimum fit to the natural data, using boundary conditions which lie entirely within the range of temperature and strain rate conditions anticipated for the Alpine Fault Zone. These results imply that the recrystallised grains measured in our samples are representative of deformation under long-term, ambient strain

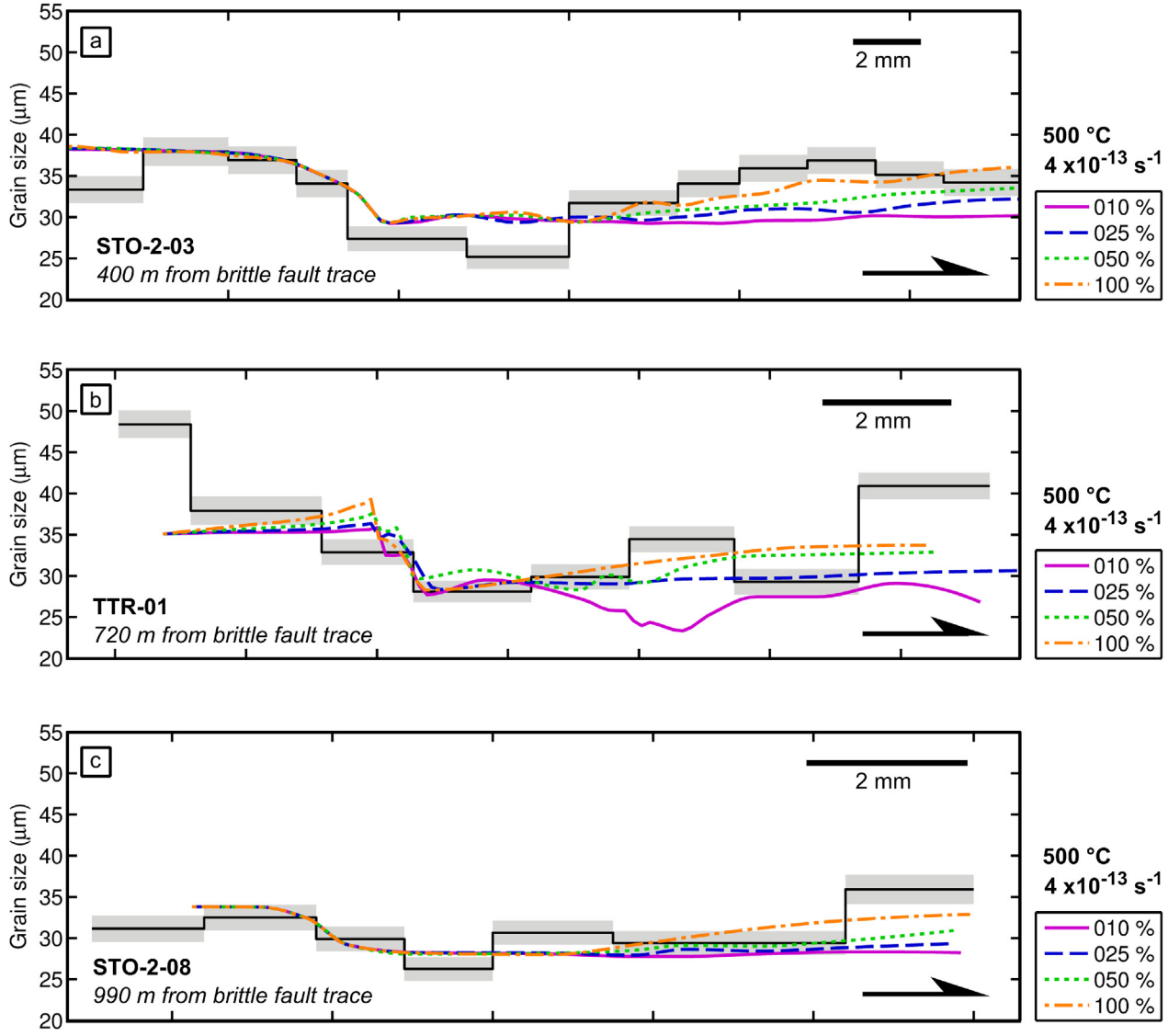

Fig. 10. Model results for each sample, using optimum strain rate and temperature boundary conditions. For each sample, the efficiency factor for grain growth, F_g has been varied to investigate the noted grain size asymmetry in each sample. Measured grain size data are shown by the solid black line, while errors of 1σ are represented by the grey shaded region.

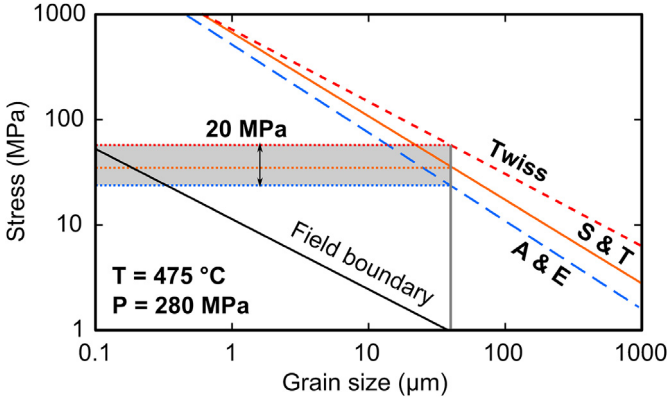

Fig. 11. A comparison of piezometers and paleowattmeters for quartz (Twiss, 1977; Stipp and Tullis, 2003; Austin and Evans, 2007) with the mechanism field boundary calculated using the Hirth et al. (2001) and Brodie and Rutter (2000) quartz flow laws for GSI and GSS creep, respectively. The grey shaded region represents the range in stress for a grain size of 40 μm, arising from differences between the piezometers and paleowattmeter.

rates, with little modification during exhumation from either seismic loading of the mid-crust or post-deformational grain growth. The high degree of agreement between model results and nature gives us confidence that this numerical method is valid for at least small scale, single phase systems. In the future, we hope to apply develop this method for studying larger, more complex (i.e. polyphase) or non-steady state systems.

Acknowledgements

This work was funded by a New Zealand Marsden Fund (UOO1116) grant awarded to D.J.P., a University of Otago Doctoral Scholarship awarded to A.J.C. and Direct Crown funding to S.E. via the Tectonics of Zealandia programme. We are grateful to Steve Kidder and Virginia Toy for early discussion and guidance, and Susanne Buiter for co-development of the SULEC finite element package. Thanks to Tim Little and Hans de Bresser for comments on an earlier version of this manuscript, and Sandra Piazolo and Marco Herwegh for constructive reviews which greatly improved the quality of this paper. Thanks also to Ian Alsop for his assistance as journal editor.

References

Austin, N.J., Evans, B., 2007. Paleowattmeters: a scaling relation for dynamically recrystallized grain size. Geology 35, 343–346.

Austin, N., Evans, B., 2009. The kinetics of microstructural evolution during deformation of calcite. J. Geophys. Res. Solid Earth 114 (1978–2012).

Bachmann, F., Hielscher, R., Schaeben, H., 2011. Grain detection from 2d and 3d EBSD data: Specification of the MTEX algorithm. Ultramicroscopy 111, 1720–1733.

Behrmann, J.H., Seckel, C., 2007. Structures, flow stresses, and estimated strain rates in metamorphic rocks of the Small Cyclades Islands Iraklia and Schinoussa (Aegean Sea, Greece). Geotect. Res. 95, 1–11.

Bercovici, D., Ricard, Y., 2005. Tectonic plate generation and two-phase damage: void growth versus grain size reduction. J. Geophys. Res. Solid Earth 110 (1978–2012).

Bercovici, D., Ricard, Y., 2012. Mechanisms for the generation of plate tectonics by two-phase grain-damage and pinning. Phys. Earth Planet. Interiors 202, 27–55.

Bercovici, D., Ricard, Y., 2013. Generation of plate tectonics with two-phase grain-damage and pinning: source–sink model and toroidal flow. Earth Planet. Sci. Lett. 365, 275–288.

Bestmann, M., Prior, D.J., Grasemann, B., 2006. Characterisation of deformation and flow mechanics around porphyroclasts in a calcite marble ultramylonite by means of EBSD analysis. Tectonophysics 413, 185–200.

Brodie, K., Rutter, E., 2000. Deformation mechanisms and rheology: why marble is weaker than quartzite. J. Geol. Soc. 157, 1093–1096.

Buiter, S., Ellis, S., 2012. SULEC: benchmarking a new ALE finite-element code. In: EGU General Assembly Conference Abstracts, p. 7528.

Cross, A., Kidder, S., Prior, D., 2015. Using microstructures and TitaniQ thermobarometry of quartz sheared around garnet porphyroclasts to evaluate microstructural evolution and constrain an Alpine Fault zone geotherm. J. Struct. Geol. 75, 17–31.

De Bresser, J.H.P., 1996. Steady state dislocation densities in experimentally deformed calcite materials: single crystals versus polycrystals. J. Geophys. Res. Solid Earth 101, 22189–22201.

De Bresser, J., Peach, C., Reijs, J., Spiers, C., 1998. On dynamic recrystallization during solid state flow: effects of stress and temperature. Geophys. Res. Lett. 25, 3457–3460.

De Bresser, J., Ter Heege, J., Spiers, C., 2001. Grain size reduction by dynamic recrystallization: can it result in major rheological weakening? Int. J. Earth Sci. 90, 28–45.

Derby, B., 1990. Dynamic recrystallization and grain size. In: Deformation Processes in Minerals, Ceramics and Rocks. Springer, pp. 354–364.

Derby, B., Ashby, M., 1987. On dynamic recrystallisation. Scr. Metall. 21, 879–884.

Ellis, S., Stöckhert, B., 2004. Imposed strain localization in the lower crust on seismic timescales. Earth Planets Space 56, 1103–1109.

Ellis, S., Little, T., Wallace, L., Hacker, B., Buiter, S., 2011. Feedback between rifting and diapirism can exhume ultrahigh-pressure rocks. Earth Planet. Sci. Lett. 311, 427–438.

Evans, B., Renner, J., Hirth, G., 2001. A few remarks on the kinetics of static grain growth in rocks. Int. J. Earth Sci. 90, 88–103.

Grigull, S., Ellis, S.M., Little, T.A., Hill, M.P., Buiter, S.J., 2012. Rheological constraints on quartz derived from scaling relationships and numerical models of sheared brittle-ductile quartz veins, central Southern Alps, New Zealand. J. Struct. Geol. 37, 200–222.

Gueydan, F., Mehl, C., Parra, T., 2005. Stress-strain rate history of a midcrustal shear zone and the onset of brittle deformation inferred from quartz recrystallized grain size. In: Geological Society, London, Special Publications, vol. 243, pp. 127–142.

Hall, C.E., Parmentier, E., 2003. Influence of grain size evolution on convective instability. Geochem. Geophys. Geosyst. 4.

Herwegh, M., Linckens, J., Ebert, A., Berger, A., Brodhag, S., 2011. The role of second phases for controlling microstructural evolution in polymineralic rocks: a review. J. Struct. Geol. 33, 1728–1750.

Herwegh, M., Poulet, T., Karrech, A., Regenauer-Lieb, K., 2014. From transient to steady state deformation and grain size: a thermodynamic approach using elasto-visco-plastic numerical modeling. J. Geophys. Res. Solid Earth 119, 900–918.

Hirth, G., Teyssier, C., Dunlap, J.W., 2001. An evaluation of quartzite flow laws based on comparisons between experimentally and naturally deformed rocks. Int. J. Earth Sci. 90, 77–87.

Humphreys, F.J., Hatherly, M., 2004. Recrystallization and Related Annealing Phenomena, vol. 416. Elsevier Oxford.

Jessell, M.W., Siebert, E., Bons, P.D., Evans, L., Piazolo, S., 2005. A new type of numerical experiment on the spatial and temporal patterns of localization of deformation in a material with a coupling of grain size and rheology. Earth Planet. Sci. Lett. 239, 309–326.

Kenkmann, T., Dresen, G., 1998. Stress gradients around porphyroclasts: palaeopiezometric estimates and numerical modelling. J. Struct. Geol. 20, 163–173.

Kidder, S., Avouac, J.P., Chan, Y.C., 2012. Constraints from rocks in the Taiwan orogen on crustal stress levels and rheology. J. Geophys. Res. Solid Earth 117 (1978–2012).

Kidder, S., Toy, V., Prior, D.J., 2014. Transient stress magnitudes in the middle crust along the Alpine Fault. In: AGU Fall Meeting Abstracts.

Kohlstedt, D., Weathers, M.S., 1980. Deformation-induced microstructures, paleopiezometers, and differential stresses in deeply eroded fault zones. J. Geophys. Res. Solid Earth 85, 6269–6285 (1978–2012).

Küster, M., Stöckhert, B., 1999. High differential stress and sublithostatic pore fluid pressure in the ductile regime– microstructural evidence for short-term postseismic creep in the Sesia Zone, Western Alps. Tectonophysics 303, 263–277.

Linckens, J., Herwegh, M., Müntener, O., Mercolli, I., 2011. Evolution of a polymineralic mantle shear zone and the role of second phases in the localization of deformation. J. Geophys. Res. Solid Earth 116 (1978–2012).

Little, T., Cox, S., Vry, J., Batt, G., 2005. Variations in exhumation level and uplift rate along the oblique-slip Alpine Fault, central Southern Alps, New Zealand. Bull. Geol. Soc. Am. 117, 707.

Masuda, T., Ando, S., 1988. Viscous flow around a rigid spherical body: a hydrodynamical approach. Tectonophysics 148, 337–346.

Mehl, L., Hirth, G., 2008. Plagioclase preferred orientation in layered mylonites: evaluation of flow laws for the lower crust. J. Geophys. Res. Solid Earth 113 (1978–2012).

Monte'si, L.G., Hirth, G., 2003. Grain size evolution and the rheology of ductile shear zones: from laboratory experiments to postseismic creep. Earth Planet. Sci. Lett. 211, 97–110.

Norris, R., Cooper, A., 2001. Late Quaternary slip rates and slip partitioning on the Alpine Fault, New Zealand. J. Struct. Geol. 23, 507–520.

Norris, R., Cooper, A., 2003. Very high strains recorded in mylonites along the Alpine Fault, New Zealand: implications for the deep structure of plate boundary faults. J. Struct. Geol. 25, 2141–2157.

Norris, R.J., Toy, V.G., 2014. Continental transforms: a view from the Alpine Fault. J. Struct. Geol. 64, 3–31.

Olgaard, D.L., Evans, B., 1986. Effect of second-phase particles on grain growth in calcite. J. Am. Ceram. Soc. 69, C-272.

Peters, M., Paesold, M., Poulet, T., Herwegh, M., Regenauer-Lieb, K., Veveakis, M., 2015. A fundamental discussion of what triggers localized deformation in geological materials. In: EGU General Assembly Conference Abstracts, p. 4495.

Piazolo, S., Bons, P., Jessell, M., Evans, L., Passchier, C., 2002. Dominance of microstructural processes and their effect on microstructural development: insights from numerical modelling of dynamic recrystallization. In: Geological Society, London, Special Publications, vol. 200, pp. 149–170.

Piazolo, S., Jessell, M., Bons, P., Evans, L., Becker, J., 2010. Numerical simulations of microstructures using the Elle platform: a modern research and teaching tool. J. Geol. Soc. India 75, 110–127.

Piazolo, S., Borthwick, V., Griera, A., Montagnat, M., Jessell, M.W., Lebensohn, R.A., Evans, L., 2012. Substructure dynamics in crystalline materials: new insight from in situ experiments, detailed EBSD analysis of experimental and natural samples and numerical modelling. In: Materials Science Forum. Trans Tech Publ., pp. 502–507.

Poirier, J.P., 1985. Creep of Crystals: High-temperature Deformation Processes in Metals, Ceramics and Minerals. Cambridge University Press.

Prior, D.J., Boyle, A.P., Brenker, F., Cheadle, M.C., Day, A., Lopez, G., Peruzzo, L., Potts, G.J., Reddy, S., Spiess, R., et al., 1999. The application of electron backscatter diffraction and orientation contrast imaging in the SEM to textural problems in rocks. Am. Mineral. 84, 1741–1759.

Ramsay, J., 1980. Shear zone geometry: a review. J. Struct. Geol. 2, 83–99.

Shigematsu, N., Prior, D., Wheeler, J., 2006. First combined electron backscatter diffraction and transmission electron microscopy study of grain boundary structure of deformed quartzite. J. Microsc. 224, 306–321.

Sibson, R., White, S., Atkinson, B., 1979. Fault rock distribution and structure within the Alpine Fault Zone: a preliminary account. Orig. South. Alps 18, 55–65.

Smith, C.S., 1948. Grains, phases, and interphases: an interpretation of microstructure. Trans. Metall. Soc. AIME 175, 15–51, 175.

Stipp, M., Tullis, J., 2003. The recrystallized grain size piezometer for quartz. Geophys. Res. Lett. 30, 2088.

Stipp, M., Tullis, J., Behrens, H., 2006. Effect of water on the dislocation creep microstructure and flow stress of quartz and implications for the recrystallized grain size piezometer. J. Geophys. Res. Solid Earth 111 (1978–2012).

Toy, V., Craw, D., Cooper, A., Norris, R., 2010. Thermal regime in the central Alpine Fault Zone, New Zealand: constraints from microstructures, biotite chemistry and fluid inclusion data. Tectonophysics 485, 178–192.

Toy, V., Norris, R., Prior, D., Walrond, M., Cooper, A., 2013. How do lineations reflect the strain history of transpressive shear zones? The example of the active Alpine Fault Zone, New Zealand. J. Struct. Geol. 50, 187–198.

Tullis, J., Yund, R., 1982. Grain growth kinetics of quartz and calcite aggregates. J. Geol. 301–318.

Twiss, R.J., 1977. Theory and applicability of a recrystallized grain size paleopiezometer. Pure Appl. Geophys. 115, 227–244.

Vry, J., Baker, J., Maas, R., Little, T., Grapes, R., Dixon, M., 2004. Zoned (Cretaceous and Cenozoic) garnet and the timing of high grade metamorphism, Southern Alps, New Zealand. J. Metamorph. Geol. 22, 137–157.

Warren, J.M., Hirth, G., 2006. Grain size sensitive deformation mechanisms in naturally deformed peridotites. Earth Planet. Sci. Lett. 248, 438–450.

White, S., 1977. Geological significance of recovery and recrystallization processes in quartz. Tectonophysics 39, 143–170.

Wightman, R., Prior, D., Little, T., 2006. Quartz veins deformed by diffusion creep-accommodated grain boundary sliding during a transient, high strain-rate event in the Southern Alps, New Zealand. J. Struct. Geol. 28, 902–918.